RADIAL ELECTRIC FIELD IN A REFLEX DISCHARGE*

Francis F. Chen
Plasma Physics Laboratory, Princeton University, Princeton, New Jersey
(Received February 12, 1962)

When a gas discharge with the electrode configuration of a Philips ionization gauge is operated in a strong magnetic field, the potential near the axis is depressed, since electrons created near the axis have difficulty crossing the magnetic field to the anode. If the magnetic field is sufficiently large, the entire discharge voltage drop is distributed radially, and there is little potential drop along the lines of force. In this case, there must be a cathode sheath drop whose magnitude varies with radius. In this paper the radial potential distribution in a hot-cathode reflex discharge is computed, and a scaling law for such discharges is obtained. Previous analyses of reflex discharges have been concerned only with the region outside the main arc column, or have neglected the cathode sheath drop, or are applicable only to cold-cathode discharges or weak magnetic fields.

The principal experimental results,[1] obtained with probes, are summarized in Fig. 1 for a discharge 300 cm long by 2.5 cm in diameter, operating with one uniformly emitting cathode and one cold cathode. The normal operating parameters were as follows: $B = 4000$ gauss, $I = 15$ amp, $V = 70$ volts, and $p = 3 \times 10^{-3}$ torr of He. This value of B is 6 or 7 times larger than that which would allow a current of 15 amperes to diffuse radially to the anode by classical collisions. Hence, a mechanism of enhanced diffusion by oscillating electric fields is probably operative. This paper is concerned only with the time-averaged properties of the discharge and not with the oscillations.[1] Furthermore, centrifugal force will be neglected, since its effect is small under the conditions of the experiment.

Figure 2 shows the idealized geometry assumed for the theory. The dashed lines indicate schematically the radially varying sheath described above. Also shown are the main particle currents: j_p is the current of primary electrons emitted by the cathode and accelerated in the sheath; j_i is the current of ions flowing to the cathode; j_{er} and j_{ir} are radial currents of electrons and ions; and j_e is the current of plasma electrons with sufficient energy to penetrate the sheath and reach the cathode. The latter current, which has been experimentally observed, has a large influence on the potential profile, and its inclusion is a novel feature of this treatment. As is apparent from the potential curve of Fig. 1, the current j_e is large near the axis and small at large radii. The con-

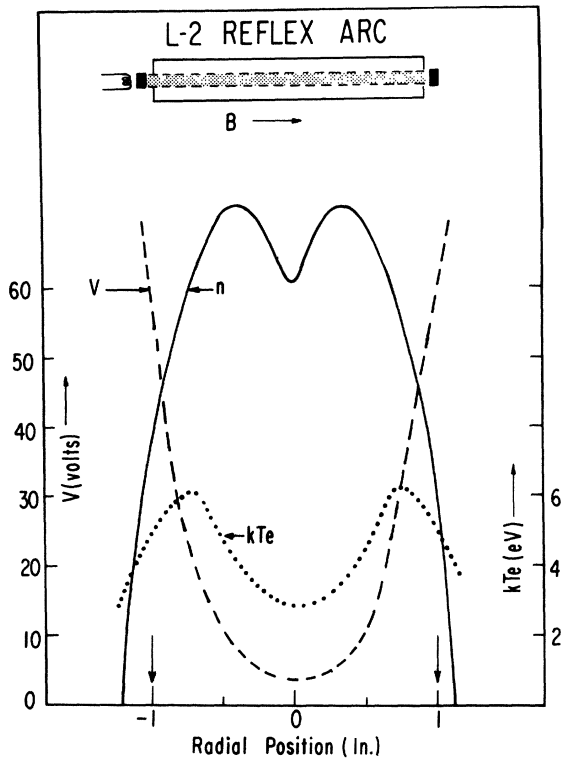

FIG. 1. Typical radial profiles of potential V, density n, and electron temperature kT_e in a reflex arc.

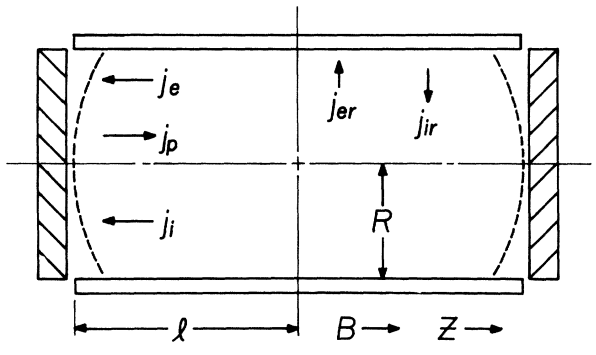

FIG. 2. Idealized geometry used for the theory, and the principal particle currents in the discharge.

comitant loss of plasma near the axis causes a dip in the density there (see Fig. 1).

We shall make the following assumptions. (1) In the plasma, $n_i = n_e$. (2) The cathode sheath can be taken into account by considering three effects: (a) All incident ions are absorbed, (b) plasma electrons are reflected according to an exponential law, and (c) primary electrons are emitted according to a law of space-charge-limited emission. (3) The discharge is cylindrically symmetric and symmetric about the mid-plane. (4) There is no plasma surrounding the discharge; that is, all particles are immediately absorbed upon reaching $r = R$. (5) Electrons are in thermal equilibrium along each line of force. (6) The temperatures kT_i and kT_e, and hence the transport coefficients, are constant. (7) The Larmor radii of all particles are small compared to R.

If $\phi = eV/kT_e$ is the normalized potential in the discharge and D, $D_\perp$, $\mu^* = |\mu| kT_e/e$, and $\mu_\perp^* = |\mu_\perp| kT_e/e$ are the longitudinal and transverse diffusion coefficients and mobilities, the equations of continuity for electrons and ions are as follows:

$$Q_e(\phi) + D_{\perp e}\nabla_r^2 n - \mu_{\perp e}^* n\nabla_r^2\phi - \mu_{\perp e}^* \frac{\partial n}{\partial r}\frac{\partial \phi}{\partial r} + D_e\frac{\partial^2 n}{\partial z^2} - \mu_e^* n\frac{\partial^2\phi}{\partial z^2} - \mu_e^*\frac{\partial n}{\partial z}\frac{\partial\phi}{\partial z} = 0, \tag{1}$$

$$Q_i(\phi) + D_{\perp i}\nabla_r^2 n + \mu_{\perp i}^* n\nabla_r^2\phi + \mu_{\perp i}^*\frac{\partial n}{\partial r}\frac{\partial\phi}{\partial r} + D_i\frac{\partial^2 n}{\partial z^2} + \mu_i^* n\frac{\partial^2\phi}{\partial z^2} + \mu_i^*\frac{\partial n}{\partial z}\frac{\partial\phi}{\partial z} = 0.$$

Here Q_e and Q_i are the source terms for electrons and ions, and the other terms describe the losses by radial and longitudinal diffusion and mobility. The source terms are of the form,

$$Q_e(\phi) = \frac{N}{2l} j_p [1 + M(\phi)] + P(\phi) - X,$$
$$Q_i(\phi) = \frac{N}{2l} j_p M(\phi) + P(\phi) - X, \tag{2}$$

where N is the number of emitting cathodes (either 1 or 2), M is the number of secondaries created per primary electron, P is the rate of ionization by plasma electrons, and X is the recombination rate. It is not necessary to specify the form of M, P, and X. The first term in Q_e represents the injection of primary electrons into the discharge, and its form assumes that these electrons traverse the length of the discharge many times before losing their energy. For space-charge-limited emission, j_p is given by $j_p = n_s v_e \iota(\phi)$, where $v_e = (2kT_e/\pi m)^{1/2}$, n_s is the plasma density at the sheath edge, and $\iota(\phi)$ is a dimensionless function (Fig. 3) computed by the author.[2] Since ϕ is defined to be 0 at the cathodes and is almost constant along any line of force, the argument of ι is essentially the cathode sheath drop.

The z dependence of Eq. (1) can be eliminated by virtue of the experimental observation that neither n nor ϕ varies greatly with z in the body of the plasma. In this case, Eqs. (1) can be integrated with respect to z from the mid-plane to the sheath edge, or approximately, from 0 to l; the radial and source terms are then approximately constant in the integration and are merely multiplied by l. The z terms become upon integration

$$\left[D_e\frac{\partial n}{\partial z} - \mu_e^* n\frac{\partial\phi}{\partial z}\right]_l = -j_e(r),$$
$$\left[D_i\frac{\partial n}{\partial z} + \mu_i^* n\frac{\partial\phi}{\partial z}\right]_l = -j_i(r), \tag{3}$$

where j_e and j_i are just the electron and ion currents to the cathodes. The electron current is

$$j_e(r) = \tfrac{1}{2} n v_e e^{-\phi(r)}, \tag{4}$$

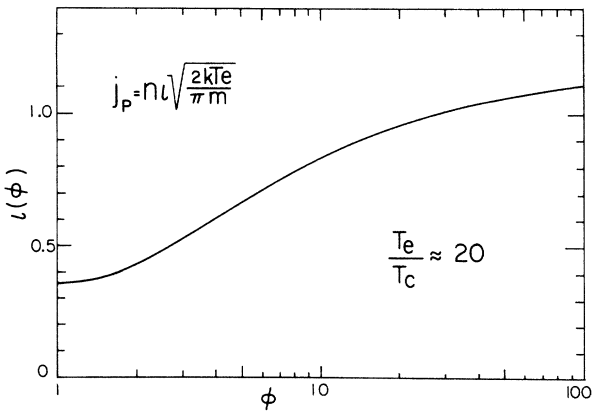

FIG. 3. Space-charge-limited emission in a plasma as a function of sheath drop.

since the electrons are in thermal equilibrium in a potential well. The ion current is given by the sheath criterion[3]:

$$j_i(r) = n_s (kT_e/M)^{1/2} \equiv n_s v_s. \tag{5}$$

Writing $\gamma = n_s/n$ and using Eqs. (3)-(5), we have for the integral of (1)

$$l\left[Q_e(\phi) + D_{\perp e}\nabla_r^2 n - \mu_{\perp e}^* n\nabla_r^2\phi - \mu_{\perp e}^* \frac{\partial n}{\partial r}\frac{\partial \phi}{\partial r}\right]$$

$$-\tfrac{1}{2}nv_e e^{-\phi} = 0, \tag{6a}$$

$$l\left[Q_i(\phi) + D_{\perp i}\nabla_r^2 n + \mu_{\perp i}^* n\nabla_r^2\phi + \mu_{\perp i}^* \frac{\partial n}{\partial r}\frac{\partial \phi}{\partial r}\right]$$

$$-\gamma n v_s = 0. \tag{6b}$$

The potential profile is obtained by subtracting Eq. (6b) from Eq. (6a), using Eq. (2) and assuming that $D_{\perp i} = D_{\perp e}$ (Bohm diffusion) and that $\mu_{\perp i}^* \gg \mu_{\perp e}^*$. One obtains

$$\tfrac{1}{2}N\gamma n v_e \iota(\phi) - l\mu_{\perp i}^*\left(n\nabla_r^2\phi + \frac{\partial n}{\partial r}\frac{\partial \phi}{\partial r}\right)$$

$$-\tfrac{1}{2}nv_e\left[e^{-\phi} - \gamma\left(\frac{2\pi m}{M}\right)^{1/2}\right] = 0. \tag{7}$$

The parameter γ is essentially the ratio of the density at the sheath edge, where the collisionless approximation applies, to that at the boundary of the collision-dominated region, where the concept of mobility applies. Since this transition region is small compared to l, ion current is conserved; and this consideration shows that γ must be of the order of 0.2 for $T_e/T_i \approx 4$. The exact value of γ, by Eq. (5), depends on the ion current, which is unknown, since ions can escape radially as well as longitudinally. Thus γ is left as an adjustable parameter. Putting r into dimensionless units, $\rho = r/R$, and dividing by $-\frac{1}{2}nv_e$, we have for (7):

$$S\left[\frac{1}{\rho}\frac{\partial}{\partial\rho}\left(\rho\frac{\partial\phi}{\partial\rho}\right) + \frac{1}{n}\frac{\partial n}{\partial\rho}\frac{\partial\phi}{\partial\rho}\right] + e^{-\phi}$$

$$-\gamma\left[N\iota(\phi) + \left(\frac{2\pi m}{M}\right)^{1/2}\right] = 0, \tag{8}$$

where

$$S = l\mu_{\perp i} e^{-1}R^{-2}(2\pi m k T_e)^{1/2} \approx lpR^{-2}B^{-2}. \tag{9}$$

The dimensionless parameter S then gives the scaling law for such discharges. Equation (8) was solved numerically for values of S corresponding to $kT_i = 0.1$, 0.3, 1.0, and 3 ev and $kT_e = 4.5$ ev, with ϕ being normalized to the experimental value at $\rho = 1$. The results are shown on Fig. 4. The term containing the density profile $d(\ln n)/d\rho$ was evaluated by using the experimental curve of Fig. 1. The effect of this term is not great, as was shown by omitting it in one run (dashed curve in Fig. 4). It is seen that good agreement with experiment both in the magnitude of $\phi(0)$ and in the shape of $\phi(\rho)$ can be obtained for reasonable values of kT_i and γ. Furthermore, the depth of the potential depression decreases with increasing S; this is the reason the radial potential variation is not dominant in discharges[4] with smaller values of R and B.

We have assumed that $\mu_{\perp i}$ is given by the classi-

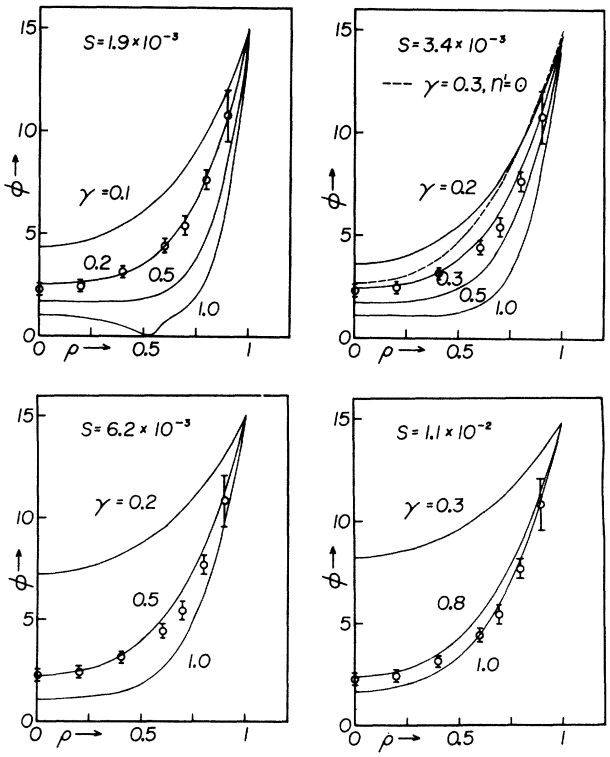

FIG. 4. The theoretical potential profiles $\phi(\rho)$ in comparison with the experimental points, for various values of γ, and for values of S corresponding to kT_i = 0.1, 0.3, 1, and 3 ev.

cal formula. If $\mu_{\perp i} = eD_{\perp i}/kT_i$, where $D_{\perp i}$ is the enhanced (Bohm) value, S becomes so large that no fit with experiment is possible. Thus an enhanced mobility is inconsistent with the assumptions we have already made.

The author is indebted to Dr. I. Rabinowitz and Mrs. H. Selberg for carrying out the numerical computation.

*This research was supported by the U. S. Atomic Energy Commission.

[1]A complete paper including the experimental details is in preparation.

[2]F. F. Chen (unpublished); but see I. Langmuir, Phys. Rev. 33, 954 (1929).

[3]D. Bohm, Characteristics of Electrical Discharges in Magnetic Fields, edited by A. Guthrie and R. K. Wakerling (McGraw-Hill Book Company, New York, 1949), Chap. 3. This proof has been verified by the author for more general boundary conditions.

[4]F. Salz, R. G. Meyerand, E. C. Lary, and A. P. Walch, Phys. Rev. Letters 6, 523 (1961).

POLARIZED NEUTRON STUDY OF ANTIFERROMAGNETIC DOMAINS IN MnF_2†

H. A. Alperin
U. S. Naval Ordance Laboratory, Silver Spring, Maryland and Brookhaven National Laboratory, Upton, New York
P. J. Brown and R. Nathans
Brookhaven National Laboratory, Upton, New York
and
S. J. Pickart
U. S. Naval Ordance Laboratory, Silver Spring, Maryland and Brookhaven National Laboratory, Upton, New York
(Received February 16, 1962)

A direct method of "seeing" antiferromagnetic domains which has not been employed heretofore is to utilize Bragg scattering of polarized neutrons from single-crystal specimens. The simplicity of this method and its sensitivity to the domain apportionment have allowed us to study the spatial distribution, temperature dependence, and response to magnetic annealing fields of the antiferromagnetic domains in MnF_2. In contrast to the recently reported technique of detecting antiferromagnetic domains by the electrically induced shift of the fluorine nuclear magnetic resonance,[1] the neutron diffraction method reported here allows one to make measurements in the very interesting region just below the Néel temperature.

A polarization dependence of the neutron scattering can be described most conveniently as a departure from unity of the ratio of the reflected intensities for incoming neutron beams of opposite polarization, i.e., $R = I_+/I_- = (N+M)^2/(N-M)^2$, where N and M are total nuclear and magnetic structure factors, respectively. For $R \neq 1$ it is clear that neither N nor M can be zero. If this condition is to be satisfied for a reflection from an antiferromagnetic structure, magnetic atoms with opposite spins must be related by one of the symmetry elements of the space group and not by a lattice translation; this requirement is satisfied for the structures shown schematically in Figs. 1(a) and 1(b) but not for the structure shown in Fig. 1(c). Secondly, there is no polarization dependence if the nuclear and magnetic structure factors are 90° out of phase. This is true when the magnetic atoms that are related by a center of symmetry have oppositely directed spins, as, for example, the case of Cr_2O_3. In MnF_2 the two Mn atoms that form the antiferromagnetic sublattices are related by a translation of $\frac{1}{2}, \frac{1}{2}, \frac{1}{2}$, but the local symmetry of the F atoms about these two sites is orthorhombic and differs by a 90° rotation about the [001] axis. Because of these

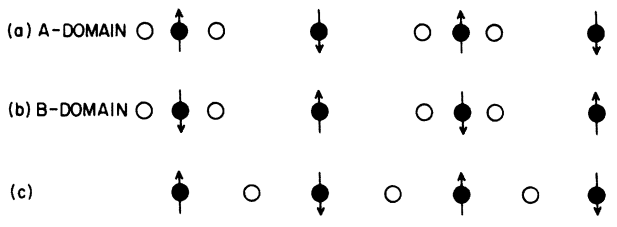

FIG. 1. One-dimensional antiferromagnetic arrays. The solid and open circles denote magnetic and nonmagnetic atoms, respectively; the arrows give the spin direction. Cases (a) and (b) will each scatter neutrons of opposite polarization differently. Case (c) is insensitive to neutron polarization.

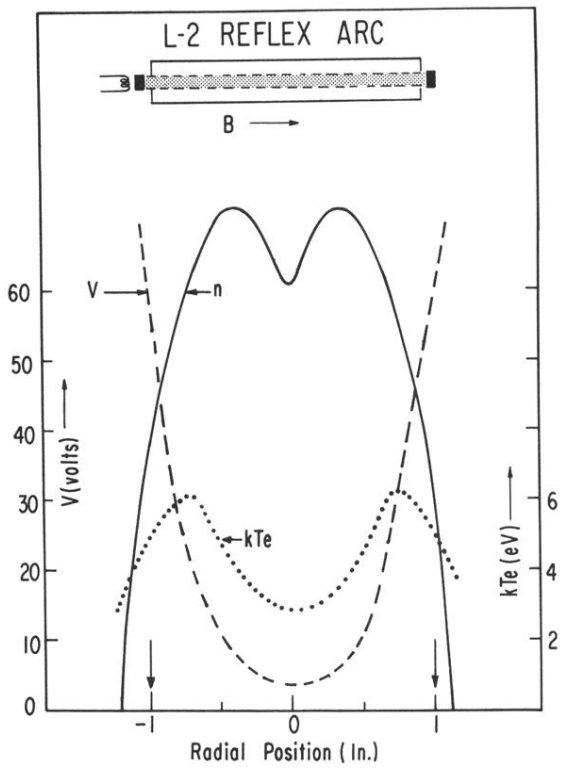

FIG. 1. Typical radial profiles of potential V, density n, and electron temperature kT_e in a reflex arc.